Numerical modeling of highly doped Si:P emitters based on Fermi–Dirac statistics and self-consistent material parameters

Pietro P. Altermatt
Centre for Photovoltaic Engineering, University of New South Wales, Sydney 2052, Australia and Inianga Consulting, 92/125 Oxford Street, Bondi Junction NSW 2022, Australia

Jürgen O. Schumacher
Fraunhofer Institute for Solar Energy Systems (ISE), Heidenhofstrasse 2, 79110 Freiburg, Germany

Andres Cuevas and Mark J. Kerr
Faculty of Engineering and IT, Australian National University, Canberra ACT 0200, Australia

Stefan W. Glunz
Fraunhofer Institute for Solar Energy Systems (ISE), Heidenhofstrasse 2, 79110 Freiburg, Germany

Richard R. King
Spectrolab Inc., 12500 Gladstone Avenue, Sylmar, California 91342

Gernot Heiser[a)]
Centre for Photovoltaic Engineering, University of New South Wales and School of Computer Science and Engineering, University of New South Wales, Sydney, 2052, Australia

Andreas Schenk
Integrated Systems Laboratory, ETH Zurich, Gloriastrasse 35, 8092 Zurich, Switzerland

(Received 25 February 2002; accepted for publication 28 June 2002)

We have established a simulation model for phosphorus-doped silicon emitters using Fermi–Dirac statistics. Our model is based on a set of independently measured material parameters and on quantum mechanical calculations. In contrast to commonly applied models, which use Boltzmann statistics and apparent band-gap narrowing data, we use Fermi–Dirac statistics and theoretically derived band shifts, and therefore we account for the degeneracy effects on a physically sounder basis. This leads to unprecedented consistency and precision even at very high dopant densities. We also derive the hole surface recombination velocity parameter S_{po} by applying our model to a broad range of measurements of the emitter saturation current density. Despite small differences in oxide quality among various laboratories, S_{po} generally increases for all of them in a very similar manner at high surface doping densities N_{surf}. Pyramidal texturing generally increases S_{po} by a factor of five. The frequently used forming gas anneal lowers S_{po} mainly in low-doped emitters, while an aluminum anneal (Al deposit followed by a heat cycle) lowers S_{po} at all N_{surf}. © *2002 American Institute of Physics.* [DOI: 10.1063/1.1501743]

I. PURPOSE OF THIS WORK

The electronics industry has, for some time, been using advanced numerical modeling for developing and optimizing devices very successfully. In contrast, one of its fastest growing branches, solar cell manufacturing, uses computer simulations only sparingly. This is partly so because common simulation techniques reproduce two of the most important device regions inadequately. First, many types of commercially manufactured silicon cells contain highly doped device regions that are performance limiting: an n^+ emitter and a p^+ backsurface field. These regions are commonly modeled with Boltzmann statistics, although Fermi–Dirac statistics should be applied instead, because Pauli-blocking reduces the *p-n* product significantly. To compensate for this lack, theories have been developed that use apparent band-gap narrowing or other effective parameters, although it has been shown on mathematically rigorous grounds that such adjustments lead to various inconsistencies.[1,2] Hence, common simulations adjust the quasi-Fermi level of minority carriers only imprecisely in such device parts.[1–4] Second, the backsurface field of many commercial cells is aluminum doped but is modeled with the intrinsic density-of-states. Aluminum forms an impurity band which is particularly far away from the valence band edge. Neglecting this leads to the wrong adjustments of the (quasi-) Fermi level of majority carriers. Hence, by using Fermi–Dirac statistics, the model presented here makes modeling a more powerful tool for the development of many types of commercial solar cells. This article deals mainly with the first issue, while the second issue is partly dealt with in a separate article.[5]

When comparing a simulation model with an experiment, one needs to keep in mind that only the *total* losses in the emitter can be measured via the emitter saturation current–density J_{oe}. This makes quantifying the recombination velocity parameter S_{po} at the surface of the emitter par-

[a)]Electronic mail: g.heiser.@unsw.edu.au

 © 2002 American Institute of Physics

ticularly challenging: S_{po} needs to be separated from losses occurring in the bulk of the emitter, and this separation has been achieved only with theoretical models. As different models divide the losses in the bulk and at the surface into different proportions, the resulting S_{po} is model dependent. This restricted approach has been used steadily, although surface recombination losses limit the efficiency in many types of solar cells.

In the past, various models have been used to extract S_{po} from J_{oe}. As outlined above, the commonly applied models use effective parameters to compensate for the incorrect statistics. In this article, however, we establish a parameter set for the use of Fermi–Dirac statistics, and we reevaluate the J_{oe} measurements made by Cuevas *et al.*,[6–8] Glunz *et al.*,[9] Kerr *et al.*,[10,11] and King *et al.*[12] We apply the band-gap narrowing model recently developed by Schenk[13] on quantum mechanical principles, and use the silicon parameter-set established by Altermatt *et al.*[14–25] Preliminary results of this project were published in Refs. 24 and 26.

II. FERMI–DIRAC STATISTICS

Most published calculations for solar cells are based on Boltzmann statistics, although it was established in the early days of semiconductor physics that Fermi–Dirac statistics need to be applied for dopant densities $N_{\mathrm{dop}} \gtrsim 1 \times 10^{19}\ \mathrm{cm}^{-3}$. Boltzmann statistics are popular because the performance-limiting parts of high-efficiency cells have been doped lower than $1\times 10^{19}\ \mathrm{cm}^{-3}$, and Fermi–Dirac (FD) statistics are cumbersome to include in analytical models. An outcome of this is that physical parameters, such as band-gap narrowing, have been extracted from experiments using Boltzmann statistics as well. This enforced the subsequent use of Boltzmann statistics, because such a parameter set partly compensated for the incorrect statistics. However, many commercial solar cells contain performance-limiting regions with $N_{\mathrm{dop}} \gtrsim 1\times 10^{19}\ \mathrm{cm}^{-3}$, where Pauli-blocking becomes significant. We therefore use FD statistics, which can be applied in numerical modeling without difficulties. This makes it necessary to adapt those parameters to FD statistics that have been commonly extracted from experiments using Boltzmann statistics.

In analogy to the law of mass action for ideal gases, the well-known relation $n_i^2 = pn$ between the intrinsic carrier density n_i and the electron and hole densities, n and p, holds only if the carriers do not interact strongly with each other, i.e., in intrinsic and moderately doped silicon. In heavily doped n-type silicon, we calculate n using

$$n = N_c F_{1/2}\left(\frac{E_{fn} - E_c^{(0)} + \Delta E_c}{kT}\right), \tag{1}$$

where N_c is the effective density of states in the conduction band, $F_{1/2}$ the Fermi integral of order 1/2, E_{fn} the quasi-Fermi level for electrons, $E_c^{(0)}$ the energy of the intrinsic conduction band edge, ΔE_c is the shift of the conduction band edge due to BGN, k is Boltzmann's constant, and T is the absolute temperature. We can express p in an analogous way. However, since the holes are non-degenerate in n-type emitters, the simple Boltzmann expression for p is appropriate:

$$p = N_v \exp\left(-\frac{E_{fp} - E_v^{(0)} - \Delta E_v}{kT}\right), \tag{2}$$

where the symbols have equivalent meaning as in Eq. (1) but for holes and the valence band. In order to clarify the influence of FD statistics on the simulated J_{oe}, we write the pn product in such a way that n_i^2, degeneracy, band-gap narrowing, and deviations from thermal equilibrium are separated in different factors:

$$\begin{aligned} pn &= N_c N_v \exp\left(-\frac{E_c^{(0)} - E_v^{(0)}}{kT}\right) \\ &\quad \times F_{1/2}\left(\frac{E_{fn} - E_c^{(0)} + \Delta E_c}{kT}\right) \\ &\quad \times \exp\left(-\frac{E_{fp} - E_v^{(0)} - \Delta E_v}{kT}\right)\exp\left(\frac{E_c^{(0)} - E_v^{(0)}}{kT}\right) \\ &= n_i^2 \frac{F_{1/2}\left(\frac{E_{fn} - E_c^{(0)}}{kT}\right)}{\exp\left(-\frac{E_c^{(0)} - E_{fn}}{kT}\right)} \\ &\quad \times \frac{F_{1/2}\left(\frac{E_{fn} - E_c^{(0)} + \Delta E_c}{kT}\right)}{F_{1/2}\left(\frac{E_{fn} - E_c^{(0)}}{kT}\right)} \exp\left(\frac{\Delta E_v}{kT}\right)\exp\left(\frac{E_{fn} - E_{fp}}{kT}\right) \\ &\equiv n_i^2 \times \gamma_{\mathrm{deg}} \times \gamma_{\mathrm{BGN}} \times \gamma_{\mathrm{neq}}. \end{aligned} \tag{3}$$

The degeneracy factor γ_{deg} is a measure of how much the pn product deviates from its value as an ideal gas. Only if the electrons are also nondegenerate, as is the case in low-doped n-type emitters, can we have $\gamma_{\mathrm{deg}} \to 1$ and $\gamma_{\mathrm{BGN}} \to 1$, so that $pn \to n_{i,\mathrm{eff}}^2 = n_i^2 \exp[(\Delta E_c + \Delta E_v)/kT]$, i.e., only then do Boltzmann statistics describe the situation well. To illustrate the difference between Boltzmann and FD statistics, we plot Eq. (3) in Fig. 1, as simulated in a highly doped emitter. We use FD statistics with BGN of Ref. 13, or Boltzmann statistics with BGN of Ref. 8, respectively (see below for details of these simulations). While BGN increases the pn product towards the surface of this diffused emitter, degeneracy tends to decrease it, leading to a maximum value of pn within the bulk. Such counteracting effects between BGN and carrier degeneracy cannot be adequately quantified using Boltzmann statistics and apparent BGN $\Delta E_g^{\mathrm{app}}$.[1,2] For example, since Boltzmann statistics overestimate p, $\Delta E_g^{\mathrm{app}}$ is made smaller than the actual shifts of the band edges to adjust the pn product, i.e., $\Delta E_g^{\mathrm{app}} < \Delta E_g \equiv \Delta E_c + \Delta E_v$. This is apparent, for example, in Fig. 7 of Ref. 11. This correction, in turn, lowers the band bending across the p-n junction of the device and hence the electric field. For further discussions of this topic, see Refs. 1, 2, 24, and 27.

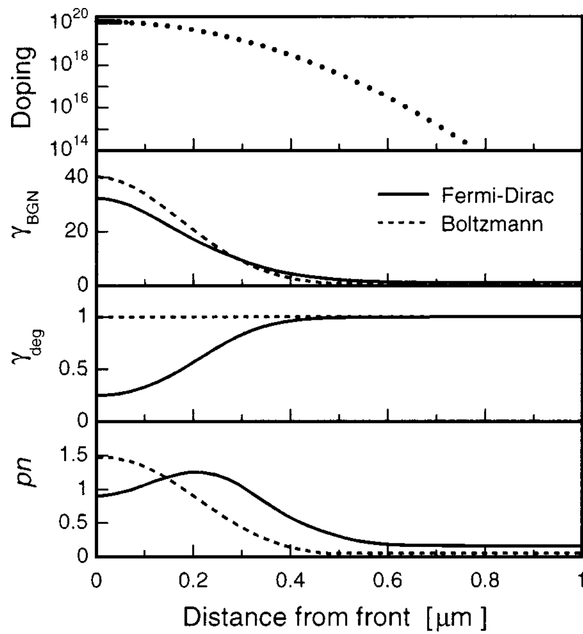

FIG. 1. Simulation of a heavily doped emitter (M4X of Ref. 12) with Boltzmann and with Fermi–Dirac statistics, respectively. Shown are the phosphorus dopant profile in units of cm^{-3}, band-gap narrowing γ_{BGN}, degeneracy γ_{deg}, and the pn product in units of 10^{33} cm^{-6}, all using Eq. (3).

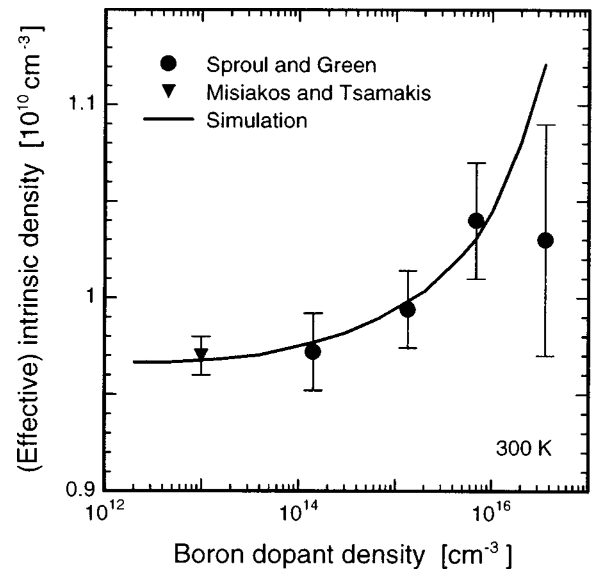

FIG. 2. (Effective) intrinsic carrier density of crystalline silicon, as a function of boron dopant density, determined by Sproul and Green (see Refs. 29 and 30) using their analytical model (circles), the value measured by Misiakos and Tsamakis (see Ref. 31) (triangle), and our simulations using $n_i = 9.65\times10^9$ cm^{-3} and the band-gap narrowing model of Ref. 13 (solid line).

III. EXPERIMENTAL FOUNDATION OF THE MODEL

In the simulation of emitters, many relevant silicon parameters and device models come into play. These are n_i, BGN, Auger recombination, the minority carrier mobility, the density of states (DOS) affected by doping, and the incomplete ionization of dopants. Apart from n_i, all of these parameters and models describe effects caused by carrier–carrier and carrier–dopant interactions. Accordingly, we can regard the improvements, made in the understanding of the highly doped Si over the past few years, as a shift from the ideal-gas model to the many-body theory. This shift needs to be experimentally substantiated, as is done in the following.

A. New intrinsic carrier density of silicon

The intrinsic carrier density is of fundamental importance since it enters into almost all calculations that relate device responses to excitations. For example, n_i strongly influences the minority carrier densities in low-doped emitters, and hence determines their J_{oe}. Prior to 1990, $n_i = 1.45\times10^{10}$ cm^{-3} was commonly used in crystalline silicon at $T = 300$ K, leading to significant deviations between the theoretically predicted and the measured behavior of devices.[28] In 1991, Green and Sproul measured $n_i = 1.00\times10^{10}$ cm^{-3},[29,30] which is significantly lower than the previously used value. This is the most widely accepted value of n_i in the silicon community. However, it has been recently shown[18,21] that the measurements of Sproul and Green were influenced by BGN, even though the dopant density of their samples was low. These recent investigations showed that n_i is slightly lower, namely $n_i = 9.65\times10^9$ cm^{-3}, which is the asymptotic value towards very low dopant densities in Fig. 2. These investigations also resolved a long prevailing discrepancy with the measurements of Misiakos and Tsamakis.[31] The important point of this article is that these recent investigations made use of a BGN model that is based on the many-body theory, where both the exchange-correlation self-energy of the free carriers and the correlation energy of the carrier–dopant interaction were treated on an equal basis.[13] Hence, we use $n_i = 9.65\times10^9$ cm^{-3} in this study.

King *et al.*[12] applied the old $n_i = 1.45\times10^{10}$ cm^{-3} for measuring J_{oe} and calculating S. Their data evaluation was revised by Cuevas *et al.*[6,8] with Sproul and Green's n_i value. Kerr *et al.*[11] and Glunz *et al.*[9] applied Sproul and Green's n_i value as well. The changes in S, caused by using the new $n_i = 9.65\times10^9$ cm^{-3} instead of Sproul and Green's value, are in most cases minor and smaller than the uncertainties imposed by the limited precision of the J_{oe} measurements.

B. Apparent versus theoretically derived band-gap narrowing

Among the material parameters and models, it has mainly been BGN that has been manipulated to compensate for the discrepancies caused by Boltzmann statistics; so we mainly need to reassess BGN when using FD statistics.

So far, solar cells have been mostly simulated with empirical BGN models that were derived from electronic measurements[25,32–43] of highly doped silicon, as is shown in Fig. 3. Absorption[44–47] and most other optical methods[48–51] yield considerably lower BGN values, as shown by the open symbols. The electronically measured apparent BGN values were extracted from transport measurements, and were influenced by the transport model involved in the data evaluation. In particular, they depended on n_i and the mobility of minority carriers μ_{min}. For example, del Alamo and Swanson[42] revised the BGN values of Fig. 3(c) mainly by adjusting the

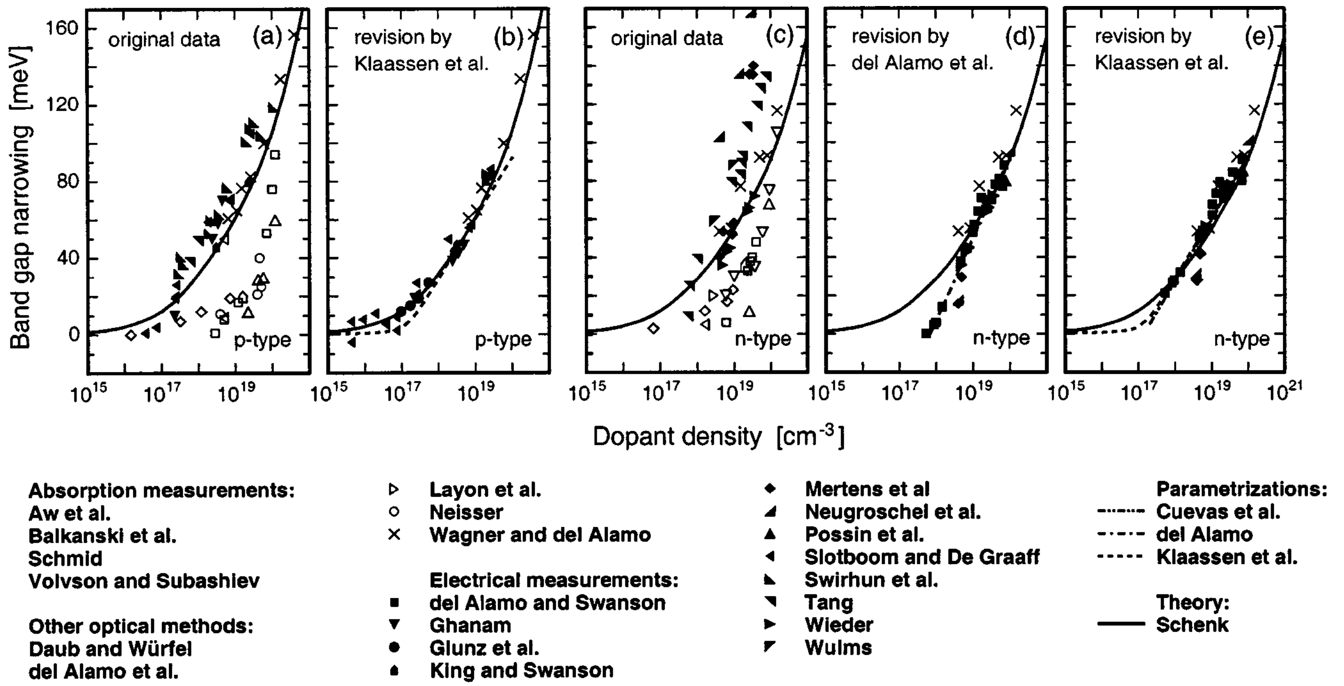

FIG. 3. Band-gap narrowing in n- and p-type silicon, measured electronically (Refs. 25, 32–43) (filled symbols), by absorption (Refs. 44–47) and other optical methods (Refs. 48–51) (open symbols), and by photoluminescence (crosses) (Ref. 52). Shown are the original data, a revision and parameterization made by del Alamo and Swanson (Ref. 42) and a revision and parameterization by Klaassen *et al.* (Ref. 32) The recent calculations (Ref. 13) (solid lines) are not apparent BGN data and therefore can only be compared with the measurements with care.

involved $\mu_{\min}$ to improved experimental results, and they obtained Fig. 3(d). However, they used the old value of n_i, so Klaassen *et al.*[32] revised the BGN values of Fig. 3(d) one time further by adjusting n_i to a lower value, with the outcome of Fig. 3(e). When n_i was adjusted to a smaller value, BGN increased at low dopant densities, because a too-high n_i value had led to compensation by a too-small BGN value. This is even more apparent in p-type silicon, as shown in Figs. 3(a) and 3(b). A reevaluation of the BGN data with $n_i = 9.65\times10^9$ cm^{-3} would shift the values in Klaassen's collection towards higher values by less than the symbol size.

Independently of these modifications, the important points here are that:

(i) These BGN values do not reflect the actual band-gap shrinkage ΔE_g, but are a conglomerate of various effects, including degeneracy[3,4,11] at high doping levels, the change in DOS due to the formation of an impurity band[2] at medium to high dopant densities, and asymmetry in gap shrinkage.[1,2,4]

(ii) Since degeneracy effects are partly compensated for in $\Delta E_g^{\rm app}$, we cannot apply Fermi–Dirac statistics together with $\Delta E_g^{\rm app}$ values, as this would overestimate the degeneracy effects.

(iii) Since the $\Delta E_g^{\rm app}$ values shown in Fig. 3 were obtained using various transport models, it is not obvious exactly how degeneracy influences $\Delta E_g^{\rm app}$, and we cannot correct the $\Delta E_g^{\rm app}$ values for FD statistics with one single and well-recognized procedure.

Instead, we choose to base our simulations on theoretically derived models, such as the comprehensive BGN model of Ref. 13. This BGN model was recently derived from a non-self-consistent, full random phase approximation (RPA) formalism at finite temperatures, where both carrier–carrier and carrier–dopant interactions were treated on an equal basis. The dispersive quasiparticle shift in RPA quality was numerically calculated and, based on these numerical results, Padé approximations of the band edge energies (ΔE_c and ΔE_v) were constructed in terms of carrier densities, dopant densities, and temperature. Since this model provides the shift of the band edge energies, it can be used together with FD statistics.

As this approach differs considerably from the determination of $\Delta E_g^{\rm app}$, we must be careful when comparing the model with $\Delta E_g^{\rm app}$ in Fig. 3. At low dopant densities and under low-level injection conditions, both carrier types are nondegenerate, and the DOS is essentially ideal. Reference 4 also shows that, under such conditions, the effects of asymmetry in BGN ($\Delta E_c \neq \Delta E_v$) are unimportant. Hence, we can directly compare the model with $\Delta E_g^{\rm app}$ under these conditions, and Figs. 3(b) and 3(e) show that there is good agreement between the two approaches. These figures also show that, compared to photoluminescence measurements[52] (shown as crosses), the model provides a similar but slightly larger ΔE_g (up to 10%) in the high doping range. This is expected because the band tails are neglected in the rigid-shift model of Ref. 13 (the approximations made in the model are discussed elsewhere[21] in more detail). However, the model is a good approximation, because band tails host immobile carriers, while n and p enter the basic semiconductor equations[53] either through the Poisson equation as charge carriers that are not electrostatically compensated, or through

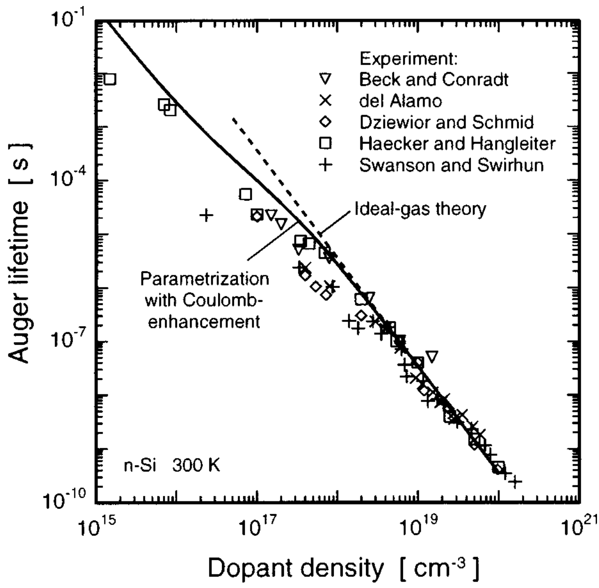

FIG. 4. Measured Auger lifetimes (Refs. 42, 54–57) at low-injection conditions, as a function of dopant density N_{dop} in n-type silicon. At $N_{\mathrm{dop}} \lesssim 10^{18}\ \mathrm{cm}^{-3}$, the lifetimes are lower than the ideal-gas limit (dashed lines) due to Coulomb enhancement (Refs. 17, 19, 59) (solid line).

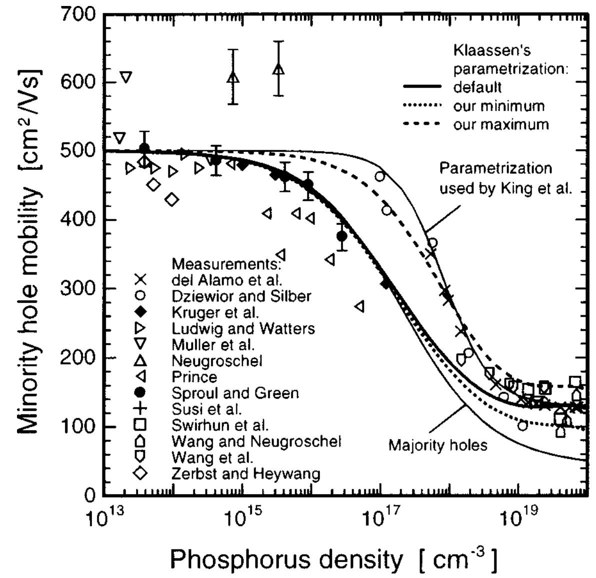

FIG. 5. Minority-carrier hole mobility $\mu_{h,\mathrm{min}}$, measured by various authors, (Refs. 35, 63–76) and parametrized by Klaassen (Ref. 77). A parameterization used in the work of King *et al.*, (Ref. 12) and a parameterization of the majority-carrier hole mobility (Ref. 93) are shown as well.

the continuity equations accounting for currents, i.e. for entirely mobile carriers. Hence, the majority carriers in immobile tail states are not expected to contribute considerably to BGN relevant to electronic devices. Similar arguments apply to the donor band at medium dopant densities. In Sec. V A we will demonstrate that the usage of FD statistics and the BGN model of Ref. 13 give consistent results.

C. Recombination losses

In many types of emitters, the dominating recombination loss occurs through the band-to-band Auger process, which is an intrinsic property of silicon. Figure 4 shows that at dopant densities $N_{\mathrm{dop}} \gtrsim 1\times10^{18}\ \mathrm{cm}^{-3}$, the measured Auger recombination lifetime[42,54–57] τ_A can be well reproduced assuming noninteracting free particles, i.e., by $\tau_A = 1/(C_n N_{\mathrm{dop}}^2)$ (see dashed line). At these dopant densities, we use the Auger coefficient $C_n = 2.8\times10^{-31}\ \mathrm{cm}^6\,\mathrm{s}^{-1}$, as reported by Dziewior and Schmid,[55] because their data show the smallest scatter of all the published lifetime data used to determine C_n.[17] In their extraction of S, Cuevas *et al.* chose a slightly different C_n value, while King *et al.* also used Dziewior and Schmid's value in the emitter.

The Auger lifetime is enhanced by Coulomb interactions at $N_{\mathrm{dop}} \lesssim 1\times10^{18}\ \mathrm{cm}^{-3}$.[17,58] A few different parameterizations of this enhancement have been published.[17,19,59] However, we will show that this enhancement influences the simulations of emitters only marginally, and it is therefore irrelevant which of the parameterizations is chosen in our simulations.

The other recombination loss is surface recombination. At the dopant densities found in emitters, it is well quantified by the Shockley–Read–Hall theory:[60,61]

$$U_s = \frac{n_s p_s - n_{i,\mathrm{eff}}^2}{S_{po}^{-1}(n_s+n_1) + S_{no}^{-1}(p_s+p_1)}, \tag{4}$$

where n_s and p_s are the electron and hole densities at the surface, which may be influenced by the surface charge density. The parameters

$$n_1 = n_{i,\mathrm{eff}} e^{(E_t - E_i)/kT} \quad p_1 = n_{i,\mathrm{eff}}^2 / n_1 \tag{5}$$

relate the energy level of the defect E_t to the intrinsic energy level E_i. The recombination rate U_s is limited by holes in n-type emitters, i.e., by the recombination velocity parameter for holes S_{po}. We assume in our simulations that the bulk SRH lifetime $\tau_{\mathrm{SRH}} = 2$ ms, which is a reasonable value for high-purity float-zone material, and is independent of N_{dop}.[17] The choice of τ_{SRH} does not affect the simulations presented here.

D. Minority carrier mobility

At dopant densities found in emitters, the mobility of minority holes $\mu_{h,\mathrm{min}}$ is limited by hole-dopant interactions in a complex manner and is not well understood.[62] It is expected that at $N_{\mathrm{dop}} \gtrsim 10^{17}\ \mathrm{cm}^{-3}$, $\mu_{h,\mathrm{min}}$ is higher than the majority-carrier hole mobility $\mu_{h,\mathrm{maj}}$, because scattering by the positively charged phosphorus ions is less effective than by the negatively charged boron ions. This effect is experimentally and theoretically well established in the case of electron mobility.[22] However, in the case of hole mobility, the measured values spread significantly (see symbols in Fig. 5).[35,63–76] In the low dopant density range, the most reliable data are the photoconductance decay measurements of Sproul *et al.*[70] and the recent Shockley–Haynes measurements of Kruger *et al.*,[65] because their method yields $\mu_{h,\mathrm{min}}$ rather directly, while most other methods are more indirect. The $\mu_{h,\mathrm{min}}$ values given by del Alamo *et al.* and by Dziewior and Silber are significantly higher than theoretically expected in the range $N_{\mathrm{dop}} = 10^{17}$–$10^{18}\ \mathrm{cm}^{-3}$, and are questionable. King *et al.* relied on these values in the data evaluation of their J_{oe} measurements; we show their parameterization in

Fig. 5 as well. Also shown for comparison is a parameterization of the majority hole mobility by Masetti, Severi, and Solmi.[93] Most important to emitter J_{oe} simulations is $\mu_{h,\min}$ at $N_{\rm dop}>10^{18}$ cm^{-3}. The measurements scatter by $\pm 40\%$ in this range. We use the default setting of Klaassen's parameterization,[77] as shown in Fig. 5. Cuevas *et al.* used a very similar model. To estimate the maximum and minimum error bounds of $\mu_{h,\min}$ on J_{oe}, we have adjusted Klaassen's parameterization in some cases, as shown by the dashed lines.

The mobility affects our J_{oe} simulations significantly only in some dopant profiles, where the emitter is at the verge of being transparent;[78] i.e., where all carriers injected from the *p-n* junction may just reach the surface. In such cases, the error bounds of $\mu_{h,\min}$ determine how much surface recombination affects J_{oe}, so these error bounds provoke the largest uncertainties in our simulations. In the other emitters, where the injected carriers reach the surface easily, or cannot reach the surface at all (i.e., where there is a dead layer), $\mu_{h,\min}$ does not influence J_{oe} significantly; the uncertainties of our simulations are then induced by the error bounds related to the J_{oe} measurements.

E. Density-of-states at high doping levels

It is common in simulations to use the intrinsic density-of-states (DOS) at all dopant densities. At high $N_{\rm dop}$, however, the dopants form a band near the band edge, which shifts the Fermi level further away from the band edge than when using the intrinsic DOS at all dopant densities.[5] As E_{fn} is situated close to this donor band, the donor states are considerably occupied by electrons so that $n<N_{\rm dop}$, which is called incomplete ionization.[5,22] As these effects are biggest near the Mott transition (which occurs at $N_{\rm dop}=3.74\times 10^{18}$ cm^{-3}), they affect only lightly doped emitters. Since the donor band is rather close to the conduction band in Si:P, the effects are considerably weaker than in *p*-type Si:Al. Hence, these effects are minor compared to the error bounds of the J_{oe} measurements. We include the donor band in some lightly doped emitters in Sec. V B to demonstrate these effects.

At very high $N_{\rm dop}$, where the donor band has merged with the conduction band, both band edges are modified by tail states, which arise due to disorder.[79] Deep tail states are localized, while the shallow ones are a hybridization between localized and extended states,[80,81] and therefore they host immobile carriers. The tail state density is too small to cause a considerable amount of incomplete ionization.[5] In contrast, the valence band edge hosts only a small number of holes, so that tailing effects may be more noticeable. Pan *et al.*[82] predicted that the equilibrium hole density will increase by a factor of two due to band tails. Unfortunately, they fitted their tail density to room-temperature photoluminescence (PL) measurements,[83] neglecting effects that cause the broadening of the PL lines.[79,84,85] For these reasons, tailing affects the minority-carrier transport considerably less than proposed by Pan *et al.* Due to the lack of experimental data, we are unable to quantify the influence of the minority-band tailing on our J_{oe} simulations.

IV. SIMULATION TECHNIQUE

We use the device simulator Dessis[86] which—in contrast to some analytical models of previous studies—solves the well-known, fully coupled set of semiconductor differential equations[53] numerically and in a self-consistent way. Great care has been taken that the numerical errors stay within negligible boundaries. We apply FD statistics at 300 K, together with the models and parameters of Sec. III. The n^+pn^+ test structures were measured in Refs. 6–12 by photoconductance transient decay and quasi-steady-state photoconductance. We find it unnecessary to use transient models in our simulations, because we can draw on the general definition[24] of J_{oe},

$$J_{oe}\equiv \frac{J_n(x_e)}{n(x_e)p(x_e)-n_{i,\rm eff}^2(x_e)}\,n_{i,\rm eff}^2(x_e), \tag{6}$$

and hence need to simulate the devices only in steady-state open-circuit condition. Equation (6) shows that J_{oe} is related to the electron recombination current J_n across the *p-n* junction, and to the excess *pn* product at the edge x_e of the space charge region. We employ the effective carrier density $n_{i,\rm eff}$ instead of n_i, to account for any BGN that may be induced by the injected carriers at high-injection conditions. The BGN model of Ref. 13 accounts for carrier-induced BGN.[20]

In the experiment, most of the diode structures had no metal contacts. A numerical simulation requires at least one "contact" in order to provide a zero level for the electrostatic potential. We therefore attach a very small floating gate at the edge of our 2D domain. This gate does not influence the recombination properties in the silicon. As doping profiles, we took the SIMS or stripping-Hall data of Refs. 6–12. According to Ref. 87, the SIMS profiles represent the electrically active phosphorus density in all the emitters used in this study.

V. RESULTS

A. Verification of consistency

While we are able to base our models of BGN, Auger recombination and mobility on independent measurements, there is no method known to us that allows us to independently measure the surface recombination velocity parameter of holes, S_{po}. Hence, we must generally treat S_{po} as unknown. An exception is when J_{oe} is measured on emitters covered with a thin metal layer:[8] S_{po} of such surfaces is then limited by the thermal velocity of free carriers v_{th}, i.e., $S_{po}=1.562\times 10^7$ and $S_{no}=2.042\times 10^7$ cm/s at 300 K, independently of the crystal orientation.[86,88,89] Hence, these metal-coated samples give us the precious opportunity to verify the consistency of our applied models and material parameters.

Indeed, we are able to reproduce the measured J_{oe} values of all metal-coated emitters (i.e., at $N_{\rm dop}<2\times 10^{20}$ cm^{-3}) without any further adjustments. This is a crucial result. It demonstrates that our model is consistent, and that this study is more than another adjustment of parameters to extract S_{po} from J_{oe} measurements: it also introduces the

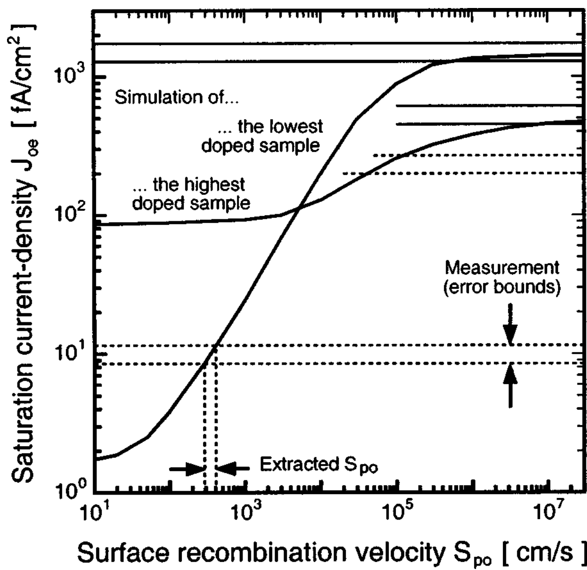

FIG. 6. Simulated saturation current–density J_{oe} of the highest and lowest doped emitter of Cuevas *et al.* (Refs. 6–8) with $N_{\text{peak}}=2.2\times10^{18}$ and 2×10^{20} cm^{-3}, respectively. The error bounds of the measured J_{oe} of metal-coated and oxide-passivated surfaces are indicated by the horizontal solid and dashed lines, respectively.

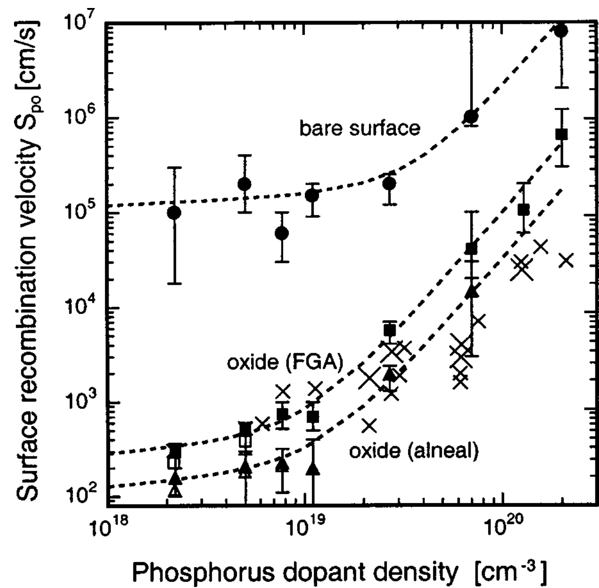

FIG. 7. Surface recombination velocity S_{po}, as extracted by our simulations from the J_{oe} measurements made by Cuevas *et al.* (Refs. 6–8) (symbols). The data obtained by their model, using Boltzmann statistics, are shown as crosses. The dashed lines are a parameterization with Eq. (7).

physically sound statistics. With previous models, such consistency has not been achieved at high N_{dop}, mainly because Boltzmann statistics were applied.

Figure 6 shows the simulated J_{oe} of both the lowest and the highest doped emitter in the collection of Cuevas *et al.*, where the doping density at the surface N_{surf} is 2.2×10^{18} and 2×10^{20} cm^{-3}, respectively. The simulated J_{oe} approaches the measured values (horizontal solid lines) when S_{po} approaches v_{th}. With Boltzmann statistics, J_{oe} would overshoot the measured values in the highly doped emitter. Generally, the simulated J_{oe} depends with varying sensitivity on S_{po}. For example, the bulk losses are large in the highly doped sample and dominate J_{oe} at $S_{po}<1000$ cm/s, so the simulated J_{oe} curve flattens out towards low S_{po}. Towards high S_{po} values, the surface recombination rate becomes limited by the hole current injected from the *p-n* junction, hence J_{oe} flattens out again.

B. Extraction of the surface recombination velocity

After having verified its consistency, we use our model to extract S_{po} from the J_{oe} measurements; S_{po} is an important material parameter in devices with passivated surfaces. Figure 6 indicates that J_{oe} is far more sensitive to S_{po} in a low doped than in a highly doped emitter (of comparable junction depth). Accordingly, we are able to extract S_{po} more precisely in some emitters than in others. For example, Fig. 6 also shows the measured J_{oe} values of devices with oxide-passivated surfaces (dashed lines). The simulated J_{oe} drops more steeply near the measured J_{oe} value in the low-doped emitter, and hence the error bounds of the extracted S_{po} are smaller than in the case of the highly doped emitter. In some cases, the error bounds of $\mu_{h,\min}$ need to be added to these error bounds.

Figure 7 shows the extracted S_{po} as a function of N_{surf} of the planar emitters fabricated by Cuevas *et al.*[6–8] Their emitters had either a bare surface, or were passivated by a thermal oxide with a forming gas anneal (FGA) or with an aluminum anneal (alneal). For details of the processing and measurement conditions, see Refs. 6–8.

Figure 7 shows that towards high N_{surf}, S_{po} increases in a straight manner, regardless of which type of surface passivation has been applied (all the dashed lines in Figs. 7–11 are a parameterization introduced in Sec. V C). Cuevas *et al.* used an analytical model together with apparent BGN and

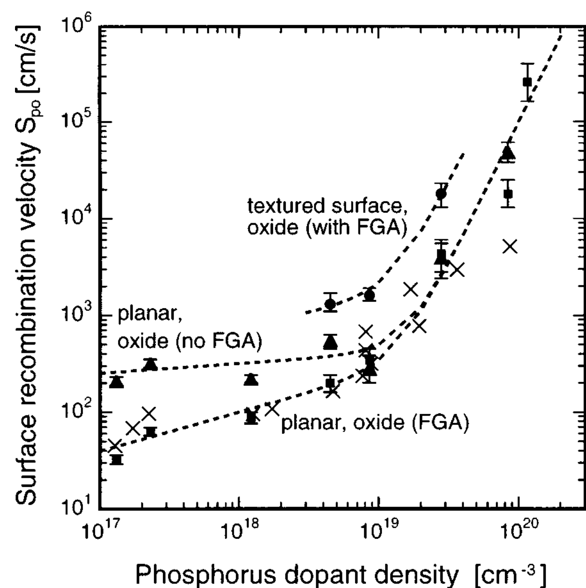

FIG. 8. Surface recombination velocity S_{po}, as extracted by our simulations from the J_{oe} measurements made by King *et al.* (Ref. 12). As these authors used the old value of the intrinsic carrier density, Cuevas *et al.* (Refs. 6–8) revised their data with the new value, still using Boltzmann statistics (crosses). The dashed lines are a parameterization with Eq. (7).

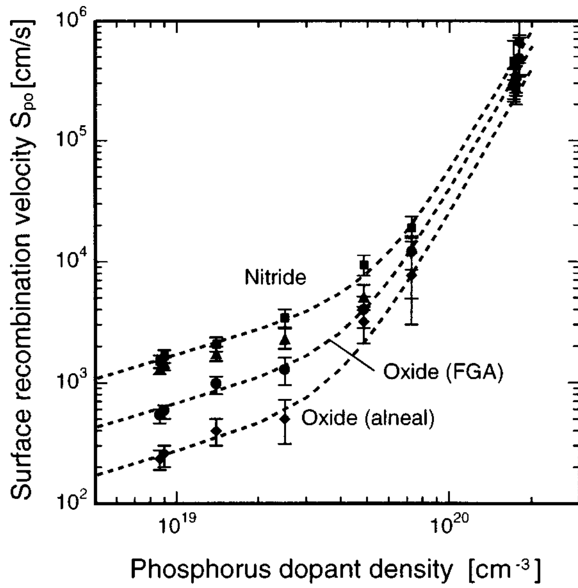

FIG. 9. Surface recombination velocity S_{po}, as extracted by our simulations from the J_{oe} measurements made by Kerr *et al.* The dashed lines are a parameterization with Eq. (7). For clarity, the parameterization of the oxide without FGA (triangles) is not shown.

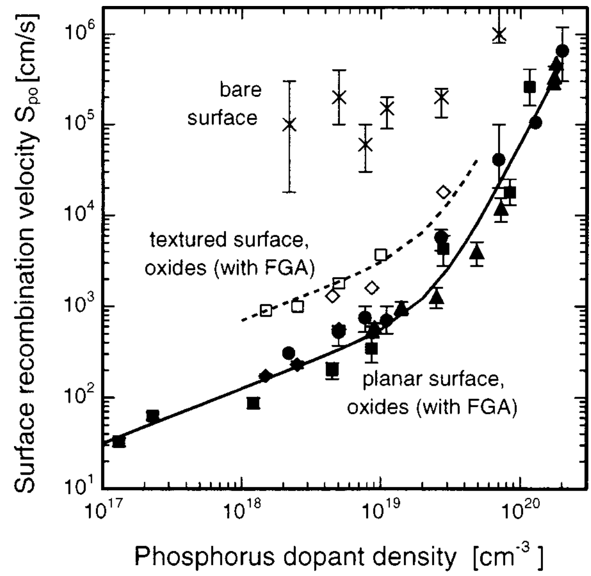

FIG. 11. Summary of Figs. 7–10, and parameterizations with Eq. (7).

Boltzmann statistics, and therefore obtained significantly lower S_{po} values at $N_{\mathrm{surf}} \gtrsim 3\times10^{19}$ cm^{-3} (indicated by the crosses in Fig. 7). As outlined in Sec. II, this was generally experienced in previous models, because degeneracy effects were not taken fully into account, leading to overestimated bulk recombination losses that were compensated with low S_{po} values (due to this compensation, previous models sometimes yielded negative S_{po} values in very highly doped emitters).

The same tendency is observed in our evaluation of the data from King *et al.*,[12] depicted in Fig. 8. For comparison, we have not plotted the original values of King *et al.* (because they were obtained using the old n_i, see Sec. III A), but rather the revised values obtained with the analytical model of Cuevas *et al.* and the new n_i. Again, our S_{po} is significantly higher at high dopant densities due to degeneracy effects.

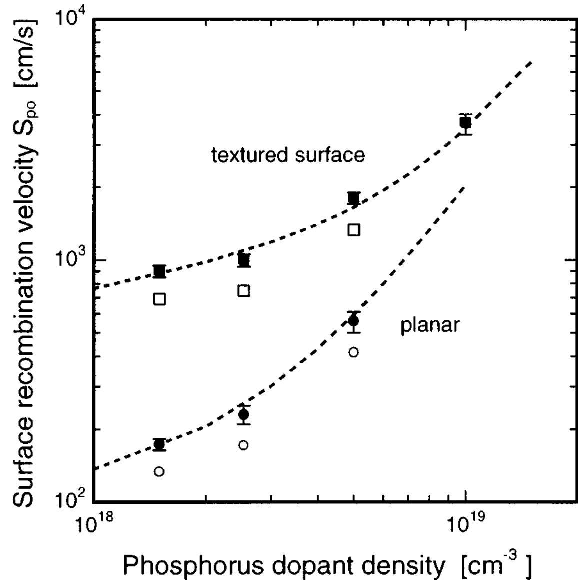

FIG. 10. Surface recombination velocity S_{po}, as extracted by our simulations from the J_{oe} measurements made by Glunz *et al.* (Ref. 9). The dashed lines are a parameterization with Eq. (7).

At the lowest N_{surf}, the injection conditions at the surface changed during the transient measurements performed by King *et al.*, and we expect J_{oe} to be injection dependent, as is commonly experienced in lightly doped rear surfaces of solar cells.[90–92] We therefore obtained the S_{po} values only from the lowest injection levels in King's experiment (in contrast, more highly doped emitters remained in very low injection conditions during the measurement, so J_{oe} is independent of the injection level).

Figure 9 shows S_{po} of the samples fabricated by Kerr *et al.*[10,11] In the case of oxide passivated surfaces, very similar behavior is found in the samples of Cuevas *et al.* and King *et al.* Kerr *et al.* also investigated PECVD silicon nitride passivation and found that it results in a higher S_{po} than does oxide passivation at all investigated dopant densities, i.e., at $N_{\mathrm{dop}} > 9\times10^{18}$ cm^{-3}. This remains in contrast to the common findings at low-doped surfaces, and suggests that the silicon nitride passivation is strongly based on electrostatic action, which works more efficiently at low dopant densities. Our analysis of the data for silicon nitride passivation includes a fixed positive oxide charge density of 2×10^{11} cm^{-2}. In comparison we use 7×10^{10} cm^{-2} at the Si/SiO$_2$ interface. The charge density has a negligible influence on our results, because the abundance of electrons in the emitters compensates for the fixed charges of the oxide or nitride layer very effectively.

So far, we have dealt with planar emitters. King *et al.* and Glunz *et al.*[9] fabricated emitters in parallel on planar and pyramidically textured wafers, and our evaluation of their measurements are shown in Figs. 8 and 10. We consider only the emitters of Glunz *et al.* that were unaffected by nonhomogeneous dopant distributions, which may be found at textured surfaces in low diffusion profiles. In both data sets, we

TABLE I. Parameters in Eq. (7) to approximate the S_{po} values shown in Figs. 7–10.

	Cuevas *et al.*			King *et al.*		
	alneal	FGA	bare	FGA	bare	textured
S_{p1}	200	450	1.5×10^5	250	400	1500
N_{p1}	1×10^{19}	1×10^{19}	1×10^{19}	1×10^{19}	1×10^{19}	1×10^{19}
γ_{p1}	0.2	0.2	0.1	0.4	0.1	0.3
S_{p2}	130	400	8000	100	100	700
N_{p2}	1×10^{19}	1×10^{19}	1×10^{19}	1×10^{19}	1×10^{19}	1×10^{19}
γ_{p2}	2.4	2.4	2.4	3	3	3
	Glunz *et al.*		Kerr *et al.*			
	textured	planar	nitride	bare oxide	FGA	alneal
S_{p1}	1500	250	1700	1400	670	270
N_{p1}	1×10^{19}	1×10^{19}	1×10^{19}	1×10^{19}	1×10^{19}	1×10^{19}
γ_{p1}	0.3	0.3	0.565	0.5	0.65	0.65
S_{p2}	2000	1800	5	4	4	2.5
N_{p2}	1×10^{19}	1×10^{19}	1×10^{19}	1×10^{19}	1×10^{19}	1×10^{19}
γ_{p2}	2.2	2.2	4	4	4	4

observe an approximately fivefold increase in S_{po} due to texturing. This increase is partly attributed to the 1.7 times larger surface area of textured compared to planar surfaces, which is not taken into account in our simulations. Partly, the increase may also be caused by the higher bond density of (111) surfaces in textured structures, compared to the (100) surface in planar surfaces.

Finally, we test by means of the lowest doped sample of Cuevas *et al.*, how strongly the Coulomb enhancement of Auger recombination affects the extraction of S_{po}. The omission of Coulomb enhancement increases the Auger losses in the bulk, and hence lowers S_{po}, but only by about 3%, and even less in more highly doped samples. These deviations are far smaller than the limitations imposed by the reproducibility of the experiments, and can be neglected.

Incomplete ionization has a slightly stronger effect in low-doped emitters, as is shown by the empty symbols in Figs. 7 and 10. However, as with the Coulomb enhancement, incomplete ionization generally has a lesser effect on S_{po} than the limitations imposed by the reproducibility of the experiments, and may be neglected as well.

C. Interpretation of the results

The S_{po} values, obtained from all the measurements, increase more gradually at low than at high dopant densities. This behavior is approximated by the following parameterization:

$$S_{po}=S_{p1}\left(\frac{N_{\mathrm{dop}}}{N_{p1}}\right)^{\gamma_{p1}}+S_{p2}\left(\frac{N_{\mathrm{dop}}}{N_{p2}}\right)^{\gamma_{p2}}. \tag{7}$$

The values of the parameters S_p (in units of cm/s), N_p (in cm^{-3}), and γ_p (a number) are given in Table I for each data set. The parameter γ_p is a measure for the slope, while both the values S_p and N_p shift S_{po} vertically, and hence are not uniquely defined; we choose $N_p=1\times10^{19}\ \mathrm{cm}^{-3}$ for all the data sets. The data of Glunz *et al.* are restricted to the transition region between N_{dop} where the first term in Eq. (7) dominates, and N_{dop} where the second term dominates. Therefore, they are most ambiguously fitted. Interestingly, the data from every group can be fitted with only one γ_{p2} for all the different passivation schemes. The values in Table I reflect that the S_{po} values vary among different authors to some extent. It is well known that the degree of surface passivation, and hence S_{po}, depends on the processing conditions and also on technological factors, some of which are difficult to control. The original references describe that different oxidation conditions (temperatures in the range 900–1000 °C) and SiO_2 thicknesses (from 13 to 105 nm) were used. In some cases, the oxide was grown *in situ* in the phosphorus diffusion furnace, while in other cases it was grown in a separate step. The presence or absence of TCA during the oxidation may also affect the results. Hence, the different data sets may indicate different degrees of surface passivation. However, these variations should not be overemphasized. Figure 11 summarizes the S_{po} values found with our improved analysis and demonstrates that the different data sets are in fact very similar. In fact, we may globally fit our planar oxidized samples that obtained a FGA with $S_{p1}=500$ and $S_{p2}=60$ cm/s, and our textured samples with $S_{p1}=2800$ and $S_{p2}=300$ cm/s. For both surface structures, we use $\gamma_{p1}=0.6$, $\gamma_{p2}=3$, and $N_{p1}=N_{p2}=1\times10^{19}\ \mathrm{cm}^{-3}$. Note that, due to the lack of data at high N_{surf}, γ_{p2} and S_{p2} are rather uncertain for textured samples. We emphasize that the surface parameters derived in this article should only be applied to device simulation if Fermi–Dirac statistics are used, together with the corresponding material parameters (such as ΔE_g instead of $\Delta E_g^{\mathrm{app}}$).

VI. CONCLUSIONS

We have established a simulation model for phosphorus-doped silicon emitters using Fermi–Dirac statistics. Our model is based on a set of independently measured material parameters and on quantum mechanical calculations. In contrast with common simulations, which use Boltzmann statistics and apparent band-gap narrowing data, we use Fermi–Dirac statistics and quantum mechanically derived band

shifts, and therefore we account for the degeneracy effects on a physically sounder basis. This leads to unprecedented consistency even at very high dopant densities, and enables us to simulate emitters with $N_{\mathrm{dop}}>3\times10^{19}\ \mathrm{cm}^{-3}$ considerably more precisely than in the past.

With our improved model, we determined the hole surface recombination velocity S_{po} by reevaluating a broad range of measurements of the emitter saturation current density. The resulting S_{po} values increase with a power-law dependence on the dopant density of the surface N_{surf}, with the trend continuing at the highest dopant densities. This contrasts common models that use Boltzmann statistics and therefore needed to compensate for the neglected degeneracy effects by apparent band-gap narrowing and reduced S_{po} values. Despite small differences in oxide quality among the various laboratories, S_{po} generally increases more gradually at low than at high dopant densities. Also, pyramidal surface texturing increases S_{po} approximately by a factor of five. The parameterization of S_{po} given here completes the physical description of highly doped Si:P required for device modeling using advanced computer simulations.

ACKNOWLEDGMENTS

P.P.A. is on a Postdoctoral Fellowship from the Australian Research Council (ARC). The Center for Photovoltaic Engineering is supported by ARC's Special Research Centres Scheme. A.C. and M.K. also acknowledge funding by the ARC.

[1] H. Kroemer, RCA Rev. **28**, 332 (1957).
[2] M. S. Lundstrom, R. J. Schwartz, and J. L. Gray, Solid-State Electron. **24**, 195 (1981).
[3] F. A. Lindholm and J. G. Fossum, IEEE Electron Device Lett. **2**, 230 (1981).
[4] A. H. Marshak, M. Ayman-Shibib, J. G. Fossum, and F. A. Lindholm, IEEE Trans. Electron Devices **28**, 293 (1981).
[5] P. P. Altermatt, A. Schenk, and G. Heiser, J. Appl. Phys. (to be published).
[6] A. Cuevas, G. Giroult-Matlakowski, P. A. Basore, C. DuBois, and R. R. King, in *Proceedings of the First World Conference on Photovoltaic Energy Conversion*, Waikoloa, HI, pp. 1446–1449.
[7] A. Cuevas, P. A. Basore, G. Giroult-Matlakowski, and C. DuBois, in *Proceedings of the 13th European Photovoltaic Solar Energy Conference, Nice, France* (H.S. Stephens, Bedford, UK, 1995), pp. 337–340.
[8] A. Cuevas, P. A. Basore, G. Giroult-Matlakowski, and C. Dubois, J. Appl. Phys. **80**, 3370 (1996).
[9] S. W. Glunz, S. Sterk, R. Steeman, W. Warta, J. Knobloch, and W. Wettling, in *Proceedings of the 13th European Photovoltaic Solar Energy Conference*, (Nice, France) (H.S. Stephens, Bedford, UK, 1995), pp. 409–412.
[10] M. J. Kerr, J. Schmidt, and A. Cuevas, in *Proceedings of the 16th EC Solar Energy Conference, Glasgow, UK* (James & James, London, 2000), pp. 1715–1718.
[11] M. J. Kerr, J. Schmidt, A. Cuevas, and J. H. Bultman, J. Appl. Phys. **89**, 3821 (2001).
[12] R. R. King, R. A. Sinton, and R. M. Swanson, IEEE Trans. Electron Devices **37**, 365 (1990).
[13] A. Schenk, J. Appl. Phys. **84**, 3684 (1998).
[14] P. P. Altermatt, G. Heiser, A. G. Aberle, A. Wang, J. Zhao, S. J. Robinson, S. Bowden, and M. A. Green, Prog. Photovoltaics **4**, 399 (1996).
[15] P. P. Altermatt, G. Heiser, X. Dai, J. Jürgens, A. G. Aberle, S. J. Robinson, T. Young, S. S. Wenham, and M. A. Green, J. Appl. Phys. **80**, 3574 (1996).
[16] P. P. Altermatt, G. Heiser, K. McIntosh, T. Kiesewetter, C. B. Honsberg, S. R. Wenham, and M. A. Green, in Proceedings of the 26th IEEE Photovoltaic Specialists Conference (Anaheim, CA, USA), pp. 179–182, IEEE, Sept. 1997.
[17] P. P. Altermatt, J. Schmidt, G. Heiser, and A. G. Aberle, J. Appl. Phys. **82**, 4938 (1997).
[18] P. P. Altermatt, A. Schenk, M. A. Green, and G. Heiser, in *Technical Digest of the 11th International Photovoltaic Science and Engineering Conference*, Sapporo, Japan (Tanaka, Kyoto, Japan, 1999), pp. 719–722.
[19] P. P. Altermatt, J. Schmidt, M. Kerr, G. Heiser, and A. G. Aberle, in *Proceedings of the 16th European Photovoltaic Solar Energy Conference, Glasgow, UK* (James & James, London, 2000), pp. 243–246.
[20] P. P. Altermatt, R. A. Sinton, and G. Heiser, Sol. Energy Mater. Sol. Cells **65**, 149 (2001).
[21] P. P. Altermatt, A. Schenk, F. Geelhaar, G. Heiser, and M. A. Green, J. Appl. Phys. (submitted).
[22] P. P. Altermatt, G. Heiser, and A. Schenk, J. Appl. Phys. (to be published).
[23] A. G. Aberle, P. P. Altermatt, G. Heiser, S. J. Robinson, A. Wang, J. Zhao, U. Krumbein, and M. A. Green, J. Appl. Phys. **77**, 3491 (1995).
[24] J. O. Schumacher, P. P. Altermatt, G. Heiser, and A. G. Aberle, Sol. Energy Mater. Sol. Cells **65**, 95 (2001).
[25] S. W. Glunz, J. Dicker, and P. P. Altermatt, Proceedings of the 17th EU Photovoltaic Energy Conference, Munich, Germany (WIP-Renewable Energies, Munich, Germany, 2001).
[26] P. P. Altermatt, J. O. Schumacher, A. Cuevas, S. W. Glunz, R. R. King, G. Heiser, and A. Schenk, in *Proceedings of the 16th EC Solar Energy Conference, Glasgow, UK* (James & James, London, 2000), pp. 102–105.
[27] A. Schenk, *Advanced Physical Models for Silicon Device Simulation* (Springer, Wien, 1998).
[28] M. A. Green, J. Appl. Phys. **67**, 2944 (1990).
[29] A. B. Sproul and M. A. Green, J. Appl. Phys. **70**, 846 (1991).
[30] A. B. Sproul and M. A. Green, J. Appl. Phys. **73**, 1214 (1993).
[31] K. Misiakos and D. Tsamakis, J. Appl. Phys. **74**, 3293 (1993).
[32] D. B. M. Klaassen, J. W. Slotboom, and H. C. de Graaff, Solid-State Electron. **35**, 125 (1992).
[33] R. R. King and R. M. Swanson, IEEE Trans. Electron Devices **38**, 1399 (1991).
[34] J. W. Slotboom and H. C. de Graaff, Solid-State Electron. **19**, 857 (1976).
[35] S. E. Swirhun, Y. H. Kwark, and R. M. Swanson, in *International Electronic Devices Meeting*, Los Angeles, CA (IEEE, New York, 1986), pp. 24–27.
[36] D. D. Tang, IEEE Trans. Electron Devices **27**, 563 (1980).
[37] R. P. Mertens, J. L. van Meerbergen, J. F. Nijs, and R. J. van Overstraeten, IEEE Trans. Electron Devices **27**, 949 (1980).
[38] A. Neugroschel, S. C. Pao, and F. A. Lindholm, IEEE Trans. Electron Devices **29**, 894 (1982).
[39] D. S. Lee and J. G. Fossum, IEEE Trans. Electron Devices **30**, 626 (1983).
[40] A. Wieder, IEEE Trans. Electron Devices **27**, 1402 (1980).
[41] H. E. J. Wulms, IEEE J. Solid-State Circuits **12**, 143 (1977).
[42] J. del Alamo and R. M. Swanson, Solid-State Electron. **30**, 1127 (1987).
[43] G. E. Possin, M. S. Adler, and B. J. Baliga, IEEE Trans. Electron Devices **31**, 3 (1984).
[44] S. E. Aw, H. S. Tan, and C. K. Ong, J. Phys.: Condens. Matter **3**, 8213 (1991).
[45] M. Balkansi, A. Aziza, and E. Amzallag, Phys. Status Solidi **31**, 323 (1969).
[46] P. E. Schmid, Phys. Rev. B **23**, 5531 (1981).
[47] A. A. Volvson and V. K. Subashiev, Sov. Phys. Semicond. **1**, 327 (1967).
[48] E. Daub and P. Würfel, J. Appl. Phys. **80**, 5325 (1996).
[49] J. A. del Alamo, R. M. Swanson, and A. Lietoila, Solid-State Electron. **26**, 483 (1983).
[50] H. P. D. Lanyon, A. K. McCurdy, and R. A. Tuft, in *Proceedings of the 13th IEEE Photovoltaic Specialists Conference, Washington, DC* (IEEE, New York, 1978), pp. 60–65.
[51] A. Neisser, Master's thesis, Institut für Festkörperphysik, Technical University of Berlin, 1998.
[52] J. Wagner and J. A. del Alamo, J. Appl. Phys. **63**, 425 (1988).
[53] W. van Roosbroeck, Bell Syst. Tech. J. **29**, 560 (1950).
[54] J. Beck and R. Conradt, Solid State Commun. **13**, 93 (1973).
[55] J. Dziewior and W. Schmid, Appl. Phys. Lett. **31**, 346 (1977).
[56] R. Häcker and A. Hangleiter, J. Appl. Phys. **75**, 7570 (1994).
[57] R. M. Swanson and S. E. Swirhun, Tech. Rep., Sandia National Laboratories, 1987, Report No. SAND97-7019.
[58] A. Hangleiter and R. Häcker, Phys. Rev. Lett. **65**, 215 (1990).
[59] M. J. Kerr and A. Cuevas, J. Appl. Phys. **91**, 2473 (2002).
[60] W. Shockley and W. Read, Phys. Rev. **87**, 835 (1952).
[61] R. Hall, Phys. Rev. **87**, 387 (1952).
[62] A. Schenk, J. Appl. Phys. **79**, 814 (1996).

[63] J. del Alamo, S. Swirhun, and R. M. Swanson, in *International Electron Devices Meeting, Washington DC* (IEEE, New York, 1985), pp. 290–293.
[64] J. Dziewior and D. Silber, Appl. Phys. Lett. **35**, 170 (1979).
[65] B. Krüger, T. Friese, F. El-Ratel, W. Sharabati, and H. G. Wagemann, Solid-State Electron. **39**, 897 (1996).
[66] G. W. Ludwig and R. L. Watters, Phys. Rev. **101**, 1699 (1956).
[67] J. Müller, H. Bernt, and H. Reichl, Solid-State Electron. **21**, 999 (1978).
[68] A. Neugroschel, IEEE Electron Device Lett. **6**, 425 (1985).
[69] M. B. Prince, Phys. Rev. **93**, 1204 (1954).
[70] A. B. Sproul, M. A. Green, and A. W. Stephens, J. Appl. Phys. **72**, 4161 (1992).
[71] E. Susi, L. Passari, M. Merli, and M. C. Carotta, Phys. Status Solidi A **106**, 583 (1988).
[72] S. E. Swirhun, J. A. del Alamo, and R. M. Swanson, IEEE Electron Device Lett. **7**, 168 (1986).
[73] C. H. Wang and A. Neugroschel, IEEE Trans. Electron Devices **11**, 576 (1990).
[74] C. H. Wang, K. Misiakos, and A. Neugroschel, Appl. Phys. Lett. **57**, 159 (1990).
[75] C. H. Wang, K. Misiakos, and A. Neugroschel, IEEE Trans. Electron Devices **37**, 1314 (1990).
[76] M. Zerbst and W. Heywang, Z. Naturf. A **11**, 608 (1956).
[77] D. B. M. Klaassen, Solid-State Electron. **35**, 953 (1992).
[78] J. A. del Alamo and R. M. Swanson, IEEE Trans. Electron Devices **31**, 1878 (1984).
[79] M. H. Cohen, M. Y. Chou, E. N. Ecoonomou, S. Jahn, and C. M. Soukoulis, IBM J. Res. Dev. **32**, 82 (1988).
[80] J. Serre and A. Ghazali, Phys. Rev. B **28**, 4704 (1983).
[81] A. Ghazali and J. Serre, Solid-State Electron. **28**, 145 (1985).
[82] Y. Pan, S. C. Jain, M. Kleffstra, and P. Balk, Solid-State Electron. **35**, 791 (1992).
[83] Y. Pan, J. Appl. Phys. **70**, 838 (1991).
[84] C. H. Grein and S. John, Phys. Rev. B **36**, 7457 (1987).
[85] M. Levy, P. Y. Yu, Y. Zhang, and M. P. Sarachik, Phys. Rev. B **49**, 1677 (1994).
[86] S. Integrated Systems Engineering, AG, Zurich, Dessis manual version 6.1, 2000.
[87] G. Masetti, D. Nobili, and S. Solmi, in *Semiconductor Silicon 1977, Proceedings of the Third International Symposium on Silicon Materials Science and Technology* edited by H. R. Huff and E. Sirtl (The Electrochemical Society, 1977), pp. 648–657.
[88] G. Ottaviani, L. Reggiani, C. Canali, F. Nava, and A. Alberigi-Quaranta, Phys. Rev. B **12**, 3318 (1975).
[89] C. Canali, C. Jacoboni, F. Nava, G. Ottaviani, and A. Alberigi-Quaranta, Phys. Rev. B **12**, 2265 (1975).
[90] S. J. Robinson, S. R. Wenham, P. P. Altermatt, A. G. Aberle, G. Heiser, and M. A. Green, J. Appl. Phys. **78**, 4740 (1995).
[91] A. G. Aberle, S. Glunz, and W. Warta, J. Appl. Phys. **71**, 4422 (1992).
[92] S. W. Glunz, A. B. Sproul, W. Warta, and W. Wettling, J. Appl. Phys. **75**, 1611 (1994).
[93] G. Masetti, M. Severi, and S. Solmi, IEEE Trans. Electron Devices **30**, 764 (1983).